


Nonequilibrium generation of charge defects in kagome spin ice under slow coolingZhijie Fan ^{1,2,3,4} and Gia-Wei Chern¹¹*Department of Physics, University of Virginia, Charlottesville, Virginia 22904, USA*²*Hefei National Research Center for Physical Sciences at the Microscale, University of Science and Technology of China, Hefei 230026, China*³*Shanghai Research Center for Quantum Science and CAS Center for Excellence in Quantum Information and Quantum Physics, University of Science and Technology of China, Shanghai 201315, China*⁴*Hefei National Laboratory, University of Science and Technology of China, Hefei 230088, China*

(Received 4 July 2023; accepted 1 May 2024; published 30 May 2024)

Kagome spin ice is one of the canonical examples of highly frustrated magnets. The effective magnetic degrees of freedom in kagome spin ice are Ising spins residing on a two-dimensional network of corner-sharing triangles. Due to strong geometrical frustration, nearest-neighbor antiferromagnetic interactions on the kagome lattice give rise to a macroscopic number of degenerate classical ground states characterized by ice rules. Elementary excitations at low temperatures are defect-triangles that violate the ice rules and carry an additional net magnetic charge relative to the background. We perform large-scale Glauber dynamics simulations to study the nonequilibrium dynamics of kagome ice under slow cooling. We show that the density of residual charge defects exhibits a power-law dependence on the quench rate for the class of algebraic cooling protocols. The numerical results are well captured by the rate equation for the charge defects based on the reaction kinetics theory. As the relaxation time of the kagome ice phase remains finite, there is no dynamical freezing as in the Kibble-Zurek scenario. Instead, we show that the power-law behavior originates from a thermal excitation that decays algebraically with time at the late stage of the cooling schedule. Similarities and differences in quench dynamics of other spin ice systems are also discussed.

DOI: [10.1103/PhysRevE.109.054133](https://doi.org/10.1103/PhysRevE.109.054133)**I. INTRODUCTION**

The nonequilibrium dynamics of many-body systems following a quench have been extensively studied over the years. Several universal behaviors after a fast quench have been established, which depend on the symmetry and conservation law of the order parameter field [1–3]. The kinetics of phase ordering following a fast quench is often governed by annihilation dynamics of topological defects in symmetry-breaking phases. On the other hand, for systems that are slowly quenched across a critical point, the Kibble-Zurek (KZ) mechanism offers a general framework for nonequilibrium dynamics and the formation of topological defects [4–7]. In particular, it shows that the excess defects left at the end of the cooling falls off with the annealing rate according to a power law whose exponent is determined by the equilibrium critical properties [8]. Originally developed to understand the density of relic topological defects in the early universe, the Kibble-Zurek mechanism has since been confirmed in phase transition dynamics of various condensed-matter systems [7,8].

The defect formation in the KZ scenario is intimately related to broken symmetries. As the order parameter in the ordered phase can take on multiple values due to the global symmetry of the system, the order parameter in general cannot be the same in regions which are beyond the equilibrium correlation length. The incompatibility of different ordered domains gives rise to topological defects, such as kinks or vortices, which are localized regions that connect two or more adjoining domains of different order parameters. A different kind of localized defects occurs in spin ices [9–12] and similar

highly constrained systems [13,14]. Due to strong geometrical frustration, spin ice remains in a disordered state at temperatures well below the dominant exchange energy scale. Yet, contrary to the uncorrelated paramagnets at high temperatures, spins in the low- T ice phase are strongly correlated. The short-range correlation is dictated by local constraints, known as the ice rules, defined on local simplex such as triangle in kagome ice and tetrahedron in pyrochlore spin ice. Importantly, violation of the ice rules gives rise to defect simplexes, which are particle-like elementary excitations of the ice phase.

Moreover, the ice rules can be formulated as the condition of minimum magnetic charges. Elementary excitations in spin ices, which are defect simplexes that violate ice rules, effectively carry an excess magnetic charge relative to the background. As these quasiparticles with a net magnetic charge are fractionalized from the fundamental dipole moments, spin ices can be viewed as a different kind of high-dimensional generalization of the one-dimensional (1D) ferromagnetic Ising model, which exhibits kink-antikink excitations fractionalized from a single-spin flip. It is worth noting that, although the 1D Ising model remains disordered at any finite temperatures, the KZ mechanism has been generalized to describe the annealing dynamics of the Ising chain when approaching its unconventional critical point at $T_c = 0$ [15–19]. The density of residual kinks after the quench is found to also exhibit a power-law dependence on annealing rates, yet with an exponent dependent on the cooling schedule. Similar studies for high-dimensional spin ice systems have yet to be carried out.

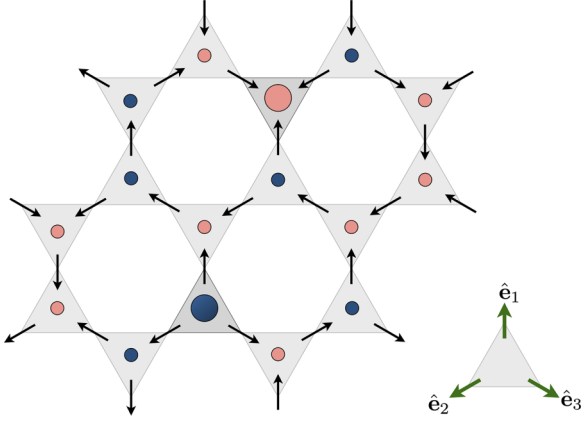


FIG. 1. Schematic of the kagome spin ice. The unit vectors \hat{e}_1 , \hat{e}_2 , and \hat{e}_3 denote the easy-axis directions of the three sublattices. The small red (light) and blue (dark) circles, indicating a magnetic charge $Q = +1$ and -1 , respectively, are triangles that satisfy ice rule constraints. The bigger red (light) and blue (dark) circles represent defect triangles with a net magnetic charge of $+3$ and -3 , respectively.

In this paper, we study the nonequilibrium dynamics of excess charge defects in short-range kagome spin ice under slow quenches. Kagome spin ice [20] is effectively an antiferromagnetic Ising model defined on the kagome lattice, a two-dimensional network of corner-sharing triangles as shown in Fig. 1. Kagome spin ices can be realized in artificial nanomagnetic systems, also known as the artificial spin ices, where elongated single domain nanomagnets, acting effectively as mesoscopic Ising spins, are arranged in a two-dimensional array and coupled via their dipolar magnetic fields [21–24]. In the case of artificial kagome spin ices, the ferromagnetic nanowires are placed at the edges of a honeycomb lattice, which is dual to the kagome lattice [25–34]. A restricted version of the kagome ice, the so-called ice-II phase, can be induced by applying a [111] magnetic field to the canonical pyrochlore spin ices such as $\text{Dy}_2\text{Ti}_2\text{O}_7$ and $\text{Ho}_2\text{Ti}_2\text{O}_7$ [35–37]. More recently, kagome ice behaviors have been observed in the tripod kagome compound $\text{Dy}_3\text{Mg}_2\text{Sb}_3\text{O}_{14}$ [38–40] and quasi-two-dimensional (quasi-2D) intermetallic compound HoAgGe [40].

As a first step toward understanding the nonequilibrium dynamics of kagome ice systems under slow quench, we focus on the antiferromagnetic kagome Ising model with interactions restricted to nearest neighbors [20]. This model by itself is an important many-body system in statistical physics. Due to the strong geometrical frustration, the spins of this model remain disordered down to zero temperature. However, at temperatures below the energy scale of the nearest-neighbor interaction, the system enters a disordered yet highly correlated liquid-like state. We perform extensive Glauber-dynamics Monte Carlo simulations of the annealing process of kagome ice. In particular, for a class of algebraic cooling schedules, the residual defects are shown to exhibit a power-law scaling with respect to the cooling rate, with an exponent dependent on the exponent of the algebraic cooling. We further adopt the reaction kinetics theory to describe the transition kinetics of triangle-simplexes in kagome ice. The results from the integration of the rate equations agree excellently with the Glauber dynamics simulations.

Contrary to standard KZ scenarios, the nearest-neighbor kagome spin ice does not exhibit a critical state at any finite or zero temperature. In fact, the relaxation time is found to be nearly temperature-independent in the ice phase. Excess defects originate from the time-varying thermal generation against a constant decay. As a result, there is no significant freezing in the annealing process. Instead, the defect density at the end of cooling results from the accumulation of excess defects within the relaxation time. This process is well captured by an analytical formula obtained from the rate equation, which gives rise to power-law scaling of residual defect density in the case of algebraic cooling protocols. Annealing dynamics in the presence of further-neighbor or long-range dipolar interactions is briefly discussed; a detailed study will be left for future studies.

The rest of the paper is organized as follows: In Sec. II, we present details of the Glauber dynamics Monte Carlo (MC) simulations for kagome spin ice and introduce parameters for algebraic cooling schedules. In Sec. III, we adapt the chemical reaction theory to describe the transition kinetics of triangle-simplexes in kagome ice and derive a rate equation for the dynamical evolution of the defect triangles. An asymptotic analytical solution for the scaling behavior in the slow cooling limit is presented in Sec. IV. Finally, a summary and outlook is presented in Sec. V.

II. GLAUBER DYNAMICS SIMULATIONS OF KAGOME SPIN ICE

Spin ices are an unusual class of frustrated ferromagnets where strong easy-axis anisotropy results in an effective antiferromagnetic Ising model defined on a lattice with corner-sharing simplexes. For kagome spin ice, the building block simplex is triangle, and the local easy-axis is along the line that connects two adjacent triangles. We introduce unit vectors \hat{e}_i to specify the easy-axis direction, which points from the center of the up-triangle to the corners. The magnetic moments are then expressed as $\mathbf{S}_i = \sigma_i \mu_0 \hat{e}_i$, where μ_0 is the magnitude of the magnetic moment, \hat{e}_i is the local crystal-field axis, and the Ising variable $\sigma_i = \pm 1$ indicates the direction of the magnetic moment.

In this work, we consider a kagome spin ice model with interactions restricted to the nearest neighbors, originally studied by Wills *et al.* [20]. Effects due to long-range dipolar interactions will be discussed in Sec. V. The geometry of the lattice is such that $\hat{e}_i \cdot \hat{e}_j = -1/2$ for any nearest-neighbor pair $\langle ij \rangle$. As a result, a ferromagnetic exchange interaction between nearest-neighbor pairs $J_F \mathbf{S}_i \cdot \mathbf{S}_j$, with $J_F < 0$, gives rise to an antiferromagnetic Ising model on the kagome lattice,

$$\mathcal{H} = J \sum_{\langle ij \rangle} \sigma_i \sigma_j = \frac{v}{2} \sum_{\alpha} Q_{\alpha}^2 + E_0, \quad (1)$$

where $J = |J_F|/2$ is the effective interaction strength. In the second equality above, the Hamiltonian is expressed in terms of magnetic charges Q_{α} associated with triangles, $v \propto J$ is an effective self-energy of charges to be determined in the following and $E_0 = NJ$ is the ground-state energy with N being the number of spins in the system. It is convenient to introduce the dumbbell representation of spin ice [41], in which magnetic dipoles are stretched into bar magnets of length ℓ

such that their poles meet at the centers of triangles. The magnetic charge associated with each pole is then $q_m = \mu_0/\ell$. One can then define a total magnetic charge for each triangle:

$$Q_\alpha = \pm q_m \sum_{i \in \alpha} \sigma_i, \quad (2)$$

where $+$ and $-$ signs are used for up- and down-triangles, respectively. The self-energy coefficient in Eq. (1) is given by $v = J\ell^2/\mu_0^2$. In the following, the magnetic charges of triangles are expressed using q_m as the unit.

The ground states of the spin ice Hamiltonian Eq. (1) are then given by states with minimum magnetic charges on every triangle. As there are three Ising spins in a triangle, the minimum charge condition is thus $Q_\alpha = +1$ or -1 , which correspond to 2-in-1-out or 1-in-2-out, respectively, spin configurations. These local constraints for the ground states are known as ice rules based on the analogy with the Bernal-Fowler rules for water ice [42]. The number of ground states satisfying these local constraints increases exponentially with the number of spins, giving rise to a finite residual entropy even at $T = 0$. The residual entropy $S_0/N = \frac{1}{3} \ln \frac{9}{2} = 0.501$ estimated by Pauling's method agrees very well with Monte Carlo simulations [20]. Importantly, the magnetic charge expression for the Hamiltonian in Eq. (1) also shows that elementary excitations in the degenerate ground-state manifold are defect triangles with a net charge $Q = +3$ or -3 , corresponding to 3-in or 3-out spin configurations, respectively.

It is worth contrasting the degenerate ice manifold of kagome with that of the pyrochlore (or its 2D checkerboard analog) spin ice. The basic simplex unit in pyrochlore is a tetrahedron with four spins. As a result, a similar minimum charge $Q = 0$ leads to the well-known 2-in-2-out ice rules. Elementary excitations of the low temperature ice phase are tetrahedra with $Q = \pm 2$, which behave as emergent magnetic monopoles in a charge-free vacuum [43]. This difference in ice rules and elementary excitations also leads to fundamentally different quench-induced nonequilibrium dynamics, which will be briefly discussed in Sec. V.

Monte Carlo method with Glauber dynamics for Ising spins [44–46] is employed to study the quench dynamics of kagome spin ice. At every time step, one random spin, say at site- i , is updated according to the transition probability

$$w(\sigma_i \rightarrow -\sigma_i; t) = \frac{1}{2} \left(1 - \tanh \frac{\beta(t)\Delta E_i}{2} \right), \quad (3)$$

where $\beta(t) = 1/T(t)$ is the time-dependent inverse temperature, and ΔE_i is the energy change due to a flipped σ_i . After each attempt of single-spin update, the simulation time t is increased by $\delta t = \tau_0/N_s$; here $N_s = 3L^2$ is the total number of spins and τ_0 is a timescale depending on the microscopic physics of the transition process.

The size-dependent time-step δt is crucial for a proper conversion from the MC simulation time to the physical time and the correct extrapolation to the thermodynamic limit [46]. As only one spin is randomly selected for update within the δt time step, the Glauber method discussed above seems to rule out the possibility of simultaneous flips of two distant spins. Physically, however, one can interpret the finite δt as a minimum timing resolution associated with finite system sizes,

which means that the interval between two consecutive spin flips is a random variable uniformly distributed between zero and δt . And as $\delta t \rightarrow 0$ in the thermodynamic limit, the above procedure properly recovers the continuous time limit. This definition of δt is also important for a proper interpretation of time-dependent quantities, as discussed in previous works [46–48].

The fundamental timescale $\tau_0 = N_s \delta t$, corresponding to the duration of N_s single-spin updates, is independent of the system size and serves as the time unit for MC simulations (which means we set $\tau_0 = 1$ in the simulations). Physically, the timescale τ_0 is given by the inverse of the microscopic transition rate of Ising spins [44]. In real materials with Ising-like spins, this fundamental transition rate τ_0^{-1} depends on the quantum tunneling mechanisms between the two microscopic states represented by the Ising variable. The physical transition rate ν for a spin-flip is $\nu \propto \tau_0^{-1} w(\sigma_i \rightarrow -\sigma_i; T)$ [44]. The temperature dependence of spin flips is controlled by the Glauber transition probability in Eq. (3).

There are three types of single-spin update which is dependent on the energy change in the transition probability: (i) $\Delta E_i = 0$ corresponding to an exchange of magnetic charges on the two triangles sharing σ_i . (ii) $\Delta E_i = \pm 4J$ due to the creation or annihilation of a single $Q = \pm 3$ defect, and (iii) $\Delta E_i = \pm 8J$ caused by the creation or annihilation of a pair of adjacent defect-triangles of opposite charges. The reaction dynamics corresponding to these spin updates are discussed in Sec. III below. At low temperatures, transitions that cost energy are dominated by the creation of single defect-triangle with $\Delta E = 4J$. For Glauber dynamics Eq. (3), this suggests a dimensionless parameter

$$\gamma(t) = \tanh [2\beta(t)J], \quad (4)$$

which is similar to the one introduced for quench dynamics of 1D Ising chain [16]. The resultant transition rate for such energy-costly process is $w(t) = \frac{1}{2}[1 - \gamma(t)]$.

The Glauber dynamics MC method is employed to investigate the temperature dependence of relaxation time $\tau(T)$ for kagome spin ice. To this end, we perform thermal quench simulations where the system is suddenly quenched from a random state to a constant low temperature at $t = 0$. All MC simulations presented in the following were performed with a linear size $L = 100$, corresponding to $N_s = 30\,000$ spins. We use n_Q to denote the density of triangles with charge Q . The defect density is given by $n_3 = (n_{+3} + n_{-3})$. The charge neutrality $n_{+3} = n_{-3}$ is preserved during the relaxation process. Figure 2 shows the decay of the density of excess defects, $\delta n_3(t) = n_3(t) - n_3^{\text{eq}}(T)$, after the quench. The resultant curves of different temperatures, after normalization by the initial value, fall nearly on the same straight line in the semilog plot, indicating an exponential decay

$$\delta n_3(t) = \delta n_3(0) e^{-t/\tau(T)}. \quad (5)$$

The estimated relaxation time is $\tau \approx 0.75$, which represents an estimate of the decay constant averaged over all temperatures. As shown by the spreading of data points at large time (e.g., $t = 8$), the relaxation time is weakly temperature dependent, with a slightly smaller value at higher temperatures.

The fact that the relaxation of charge defects is well described by an exponential decay also indicates their

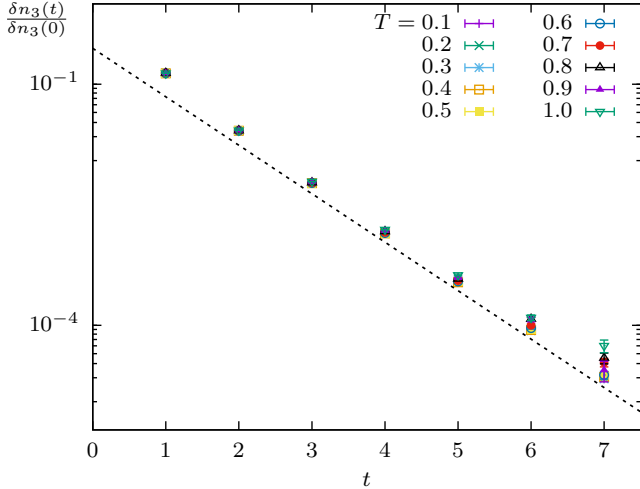


FIG. 2. Semilog plot of the normalized density of excess charge defect δn_3 versus time for kagome ice under instant quench to various temperatures. The density is normalized by the initial value of random spin configuration where the fraction of 3-in-3-out triangles is $n_3(0) = 1/4$. The dashed line shows an exponential decay $e^{-t/\tau}$ with $\tau \approx 0.75$.

non-topological nature. The dominant process of the relaxation is through the decay of, e.g., a $Q = +3$ defect into a $+1$ triangle, while converting a neighboring $Q = -1$ triangle to $+1$. Pair annihilations of ± 3 defects are negligible in the equilibration. This is in stark contrast with the case of pyrochlore spin ice where pair annihilations of $Q = \pm 2$ magnetic monopoles are the driving process of relaxation after quench, giving rise to a $1/t$ decay of excess monopole density when quenched to zero temperature [49].

The nearly temperature-independent τ of defect triangles n_3 can also be attributed to the above fact that the relaxation after a sudden quench is dominated by the spontaneous decay of defect triangles. As the energy change due to such a decay is $\Delta E = -4J$, the corresponding transition probability from Eq. (3) is $w = \frac{1}{2}[1 - \tanh(2J/T)] \approx 1$, for temperature $T \lesssim 0.5J$. As a result, the relaxation time τ shows a very weak dependence on T for low-temperature quenches, consistent with results in Fig. 2. In this limit, the physical relaxation time is essentially given by the microscopic relaxation τ_0 discussed above.

Next we apply the Glauber dynamics simulations to study the relaxation of charge defects under slow cooling. To this end, the system is prepared in an infinite- T equilibrium state at time $t = 0$. The temperature is then decreased to $T = 0$ at a time $t = \tau_Q$ according to a prescribed schedule. The inverse of the cooling time, τ_Q^{-1} , thus serves as a measure of the annealing rate. We consider a class of algebraic cooling schedules, similar to those introduced in Ref. [16] for the quench dynamics of the Ising chain. In terms of the dimensionless parameter $\gamma(t)$, the thermal-bath temperature varies with time according to

$$1 - \gamma(t) = \left(1 - \frac{t}{\tau_Q}\right)^\alpha. \tag{6}$$

In particular, the case of $\alpha = 1$ corresponds to a linear increase of γ from zero at $t = 0$ to $\gamma = 1$ at the end of cooling. Regardless of the exponent α , the physical temperature goes from $T(t = 0) = \infty$ to zero at $t = \tau_Q$. In all cases, since the temperature drops quickly in the initial stage when $t \lesssim 0.1\tau_Q$, the system is significantly out of equilibrium in this initial period. The late-stage nonequilibrium dynamics of defects is likely not affected much by this initial rapid cooling period.

For a given exponent α of the algebraic cooling schedule, Glauber dynamics simulations were performed with the cooling time $\tau_Q = 10 \times 2^m$, where $m = 0, 1, 2, \dots, 10$. Figure 3 shows the defect density $n_3(t)$ versus time for three different exponents $\alpha = 1, 2$, and 3 and varying cooling time τ_Q in both log-log and semilog plots. For $m \leq 7$, each data point was obtained by averaging results from more than 10 000 randomly generated initial states, while for $m > 7$, more than 1500 randomly generated initial states are averaged. The overall behavior is that of a slow decrease of charge defects for most of relaxation process, followed by a rather rapid drop at the end of cooling. From the semilog plots shown in Figs. 3(d)–3(f), the rapid decline of the defect density at the late stage can be approximated by an exponential decay. However, for algebraic cooling with $\alpha = 2$ and 3 , the decay of the defects slows down significantly near the end of the annealing. Importantly, the residual defect density left at $t = \tau_Q$ exhibits a power-law dependence on the cooling time

$$n_3(\tau_Q) \sim \tau_Q^{-\mu}, \tag{7}$$

where the exponent μ seems to be given by the exponent α of the algebraic cooling. These results are rather intriguing since, as demonstrated above, the relaxation time $\tau(T)$ remains rather short. Unlike 1D Ising chain or pyrochlore spin ice, the nearest-neighbor kagome spin ice does not exhibit a critical point at $T = 0$. As a result, the system does not suffer from KZ-type freezing due to critical slowing down and finite cooling rate.

III. REACTION KINETICS OF CHARGE DEFECTS

To understand the scaling behaviors of the charge defects in kagome spin ice, we adopt the reaction kinetics theory to describe the dynamical evolution of the defect triangles. The basic idea is to describe the time evolution in terms of the number densities of triangle-simplexes of different charges in a mean-field sense. For convenience, we also borrow terms from chemical reaction theory and use species to refer to triangles of different charges. Assuming that the magnet remains spatially homogeneous during relaxation, rate equations are employed to describe the “chemical reactions” of different triangle species. In kagome spin ice, there are four different species, corresponding to triangles with magnetic charge $Q = \pm 1$, and ± 3 . In terms of magnetic charges, Fig. 4 summarizes the four distinct types of processes due to a single spin-flip. The first one in Fig. 4(a) shows the exchange of $+1$ and -1 charges between two adjacent triangles. The process shown in Fig. 4(b) describes the exchange of $+3$ and $+1$ changes between nearest-neighbor triangles, which can be thought of as the diffusion of the $+3$ defect. In both cases, the energy is conserved, $\Delta E = 0$, and there is no net change in

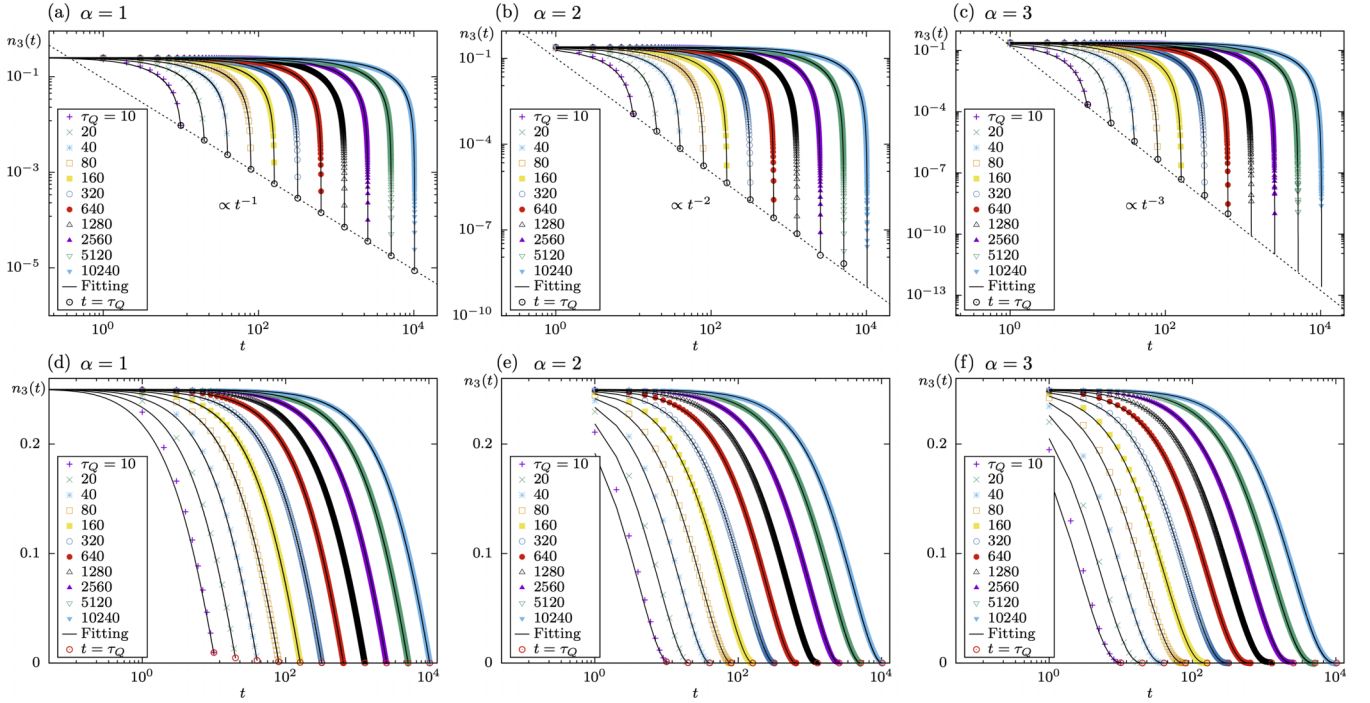


FIG. 3. Relaxation of charge defect density $n_3(t)$ as a function of time t in log-log plots for the kagome spin ice undergoing algebraic cooling schedules with (a) $\alpha = 1$ (“linear” cooling), (b) $\alpha = 2$, and (c) $\alpha = 3$ with different values of the quench time τ_Q . Panels (d)–(f) show the corresponding results in the semilog plots. The solid black curves are fitted with mean-field results with parameters $A_1 = 1.566$ and $A_2 = 0.600$. The dashed lines correspond to the analytical formula Eq. (22) obtained from the asymptotic solution of the rate equation. The final defect density $n_3(t = \tau_Q)$ (empty black circles) exhibits power-law relaxation with cooling time τ_Q .

simplex species. As a result, these two processes are similar to “physical process,” as opposed to the chemical processes to be discussed below.

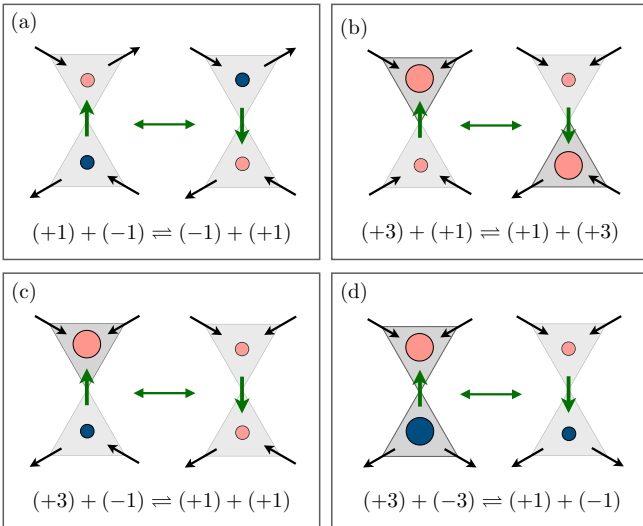
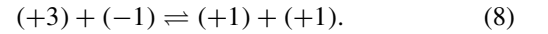
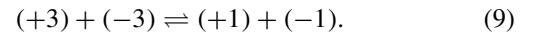


FIG. 4. Summary of simplex reactions due to a single spin-flip in kagome spin ice. The blue (dark) and red (light) circles denote positive and negative charges, respectively. (a) Exchange of +1 and -1 charges. (b) Exchange of +3 and +1 charges (and a similar one for -3 and -1). (c) Reaction of +3 and -1 into two +1 triangles (and the time-reversal counterpart). (d) Pair-annihilation of $Q = \pm 3$ charges.

The process depicted in Fig. 4(c) corresponds to the decay of a +3 defect into a +1 triangle, while shedding the extra charge to convert a neighboring -1 triangle into +1. The resultant “chemical” reaction and its reverse can be summarized as

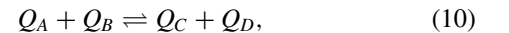


And, finally, Fig. 4(d) describes the pair-annihilation of ± 3 charge defects into ± 1 ice-rules obeying triangles, with the chemical reactions:



It is worth noting that since these reactions are induced by the flipping of a magnetic dipole, the total magnetic charge is always conserved.

Next we use chemical reaction theory to derive constraints on the reaction rates, which are required for obtaining the rate equations. To this end, we consider a general chemical reaction



where Q_A, Q_B are the initial reactants, and Q_C, Q_D are the final products. Charge conservation requires $Q_A + Q_B = Q_C + Q_D$. The two-way harpoon indicates that the reaction can occur in both forward and reversed directions. It is convenient to choose the forward direction as the one that lowers the total energy, i.e., $\Delta E < 0$. These are consistent with both reactions in Eqs. (8) and (9). In other words, the forward reaction is the decay or the annihilation of magnetic charges, while the reversed reaction is the excitation of magnetic charges.

For a given reaction, its rate is proportional to densities of the reactants. For example, the transition rate of forward reaction for Eq. (10) is $v_+ \propto n_{Q_A} n_{Q_B}$. The net rate of reaction in the forward direction is then

$$v = v_+ - v_- = k_+ n_{Q_A} n_{Q_B} - k_- n_{Q_C} n_{Q_D}, \quad (11)$$

where n_Q is the density of triangles with charge Q , and k_{\pm} denote the reaction coefficients of forward or reversed reactions, respectively. These reaction coefficients, however, are not independent. When the system reaches equilibrium, the net change is zero $v = 0$, which in turn means $k_+/k_- = n_{Q_C}^{\text{eq}} n_{Q_D}^{\text{eq}} / n_{Q_A}^{\text{eq}} n_{Q_B}^{\text{eq}}$. The equilibrium densities of the various species are given by the Boltzmann distribution, $n_Q^{\text{eq}} = g_Q e^{-\beta E_Q} / Z$, where Z is the partition function, E_Q is the energy of charge species Q , and g_Q is its degeneracy. We thus have

$$\frac{k_+}{k_-} = \frac{g_{Q_C} g_{Q_D}}{g_{Q_A} g_{Q_B}} e^{-\beta \Delta E}, \quad (12)$$

where ΔE is the energy difference between products and reactants. In general, the reaction coefficients k_{\pm} can be expressed as

$$k_{\pm} = A_{\pm} e^{-\beta \varepsilon_{\pm}}, \quad (13)$$

where ε_{\pm} are the activation energies for the forward or backward reactions, respectively. In chemical reactions which often involve an intermediate state, these energy barriers are the energy differences between the intermediate state and the initial or final state, respectively. The coefficients A_{\pm} are now nearly temperature independent. Let E^* be the energy of the intermediate state, we have $\varepsilon_+ = E^* - (E_{Q_A} + E_{Q_B})$ and $\varepsilon_- = E^* - (E_{Q_C} + E_{Q_D})$. Substitute Eq. (13) into the ratio in Eq. (12), and using the fact that $\varepsilon_+ - \varepsilon_- = \Delta E$, we obtain the ratio between the two prefactors

$$\frac{A_+}{A_-} = \frac{g_{Q_C} g_{Q_D}}{g_{Q_A} g_{Q_B}}. \quad (14)$$

The overall reaction rate, and in particular its temperature dependence, naturally also depends on the energy level E^* of the intermediate state. However, for Ising spins with Glauber dynamics, the transition rate Eq. (3) only depends on the energy difference ΔE , which does not involve any intermediate state. Or equivalently, the initial state with a higher energy serves as such intermediate, hence $\varepsilon_+ = 0$ and $\varepsilon_- = |\Delta E|$.

With these simplifications, there is only one independent parameter, e.g., A_- , for the determination of the net reaction rate

$$v = A_- \left[\frac{g_{Q_C} g_{Q_D}}{g_{Q_A} g_{Q_B}} n_{Q_A} n_{Q_B} - e^{-\beta |\Delta E|} n_{Q_C} n_{Q_D} \right]. \quad (15)$$

When a charge species is involved in multiple reactions, the rate equation of its density should include contributions from all possible reactions. For the case of defect triangles with $Q = \pm 3$, one needs to consider both the decay and the pair-annihilation. As a result, we have $dn_{+3}/dt = -v_{\text{decay}} - v_{\text{pair}}$, where v_{decay} and v_{pair} are the reaction rates of Eqs. (8) and (9), respectively. The rate equations can be further simplified by taking into account the charge neutrality conditions, $n_{+3} = n_{-3}$ and $n_{+1} = n_{-1}$, which are verified to high precision in our Glauber dynamics. We define the total density of charge

defects as $n_3 = (n_{+3} + n_{-3})$, and the density of the ground-state triangles as $n_1 = (n_{+1} + n_{-1})$. As the total number of triangles in a kagome lattice is fixed, we have $n_1 = 1 - n_3$ and only need to consider the rate equation for the density of charge defect, which is given by

$$\frac{dn_3}{dt} = A_1 (e^{-8\beta J} n_1^2 - 9n_3^2) + A_2 (e^{-4\beta J} n_1^2 - 3n_1 n_3). \quad (16)$$

The two coefficients A_1, A_2 are temperature-independent parameters to be determined by fitting with the MC simulation results. Starting from an initially random configuration where $n_3(0) = 1/4$, the above rate equation is numerically integrated using a variable step and variable order ordinary differential equation solver. By fitting the integration results with data points from one particular cooling time $\tau_Q = 160$ of the linear schedule, we obtained $A_1 = 1.566$ and $A_2 = 0.600$. Remarkably, as shown in Fig. 3, the rate equation description based on these two fitted parameters gives consistent results with the Glauber dynamics simulations for all three algebraic cooling schedules and a wide range of cooling time τ_Q . Moreover, excellent agreements were obtained not only for the residual defect density at the end of cooling, but also for the entire relaxation process.

IV. ASYMPTOTIC SOLUTION OF THE RATE EQUATION

In this section, we solve the rate equation (16) in the slow cooling limit $\tau_Q \gg \tau$, where τ is the nearly constant relaxation time in Eq. (5). At low temperatures, the defect density is small $n_3 \ll 1$, and we can approximate $n_1 = 1 - n_3 \approx 1$. This also means that the pair annihilation term in the rate equation can be neglected. Moreover, spontaneous pair creation of charge defects with an exponential factor $e^{-8\beta}$ is also negligible compared with the generation of a single defect. This means that the A_1 term, corresponding to pair creation or annihilation processes shown in Fig. 4(d), can be neglected. The rate equation then becomes

$$\frac{dn_3}{dt} = -\frac{n_3}{\tau} + \frac{1}{3\tau} e^{-4\beta(t)J}, \quad (17)$$

where the relaxation time $\tau = 1/(3A_2)$. Using numerical value $A_2 = 0.600$ fitted from the cooling simulations, we obtain $\tau \approx 0.555$, which is consistent with the estimate from the instant quench simulations shown in Fig. 2. The above equation can be readily integrated to give

$$n_3(t) = n_3(t_0) e^{-(t-t_0)/\tau} + \frac{1}{3\tau} \int_{t_0}^t e^{-4\beta(s)J} e^{-(t-s)/\tau} ds. \quad (18)$$

Here t_0 is a characteristic instant after which the low- T approximation Eq. (17) of the rate equation is valid. The residual charge defect is given by $n_3(t = \tau_Q)$. In the slow cooling limit $\tau_Q \gg \tau$, the first initial-value term with $n_3(t_0)$ tends to zero. We have

$$n_3(\tau_Q) = \frac{1}{3\tau} \int_{t_0}^{\tau_Q} e^{-4\beta(s)J} e^{-(\tau_Q-s)/\tau} ds. \quad (19)$$

This integral in the slow cooling limit is dominated by the time region $s \lesssim \tau_Q$ because of the exponentially decaying memory function $\exp[-(\tau_Q - s)/\tau]$. For convenience, we introduce a

change of variable $\eta = (\tau_Q - s)/\tau$. By expressing the Arrhenius factor $e^{-4\beta J}$ in terms of the dimensionless γ , we have

$$n_3(\tau_Q) = \frac{1}{3} \int_0^{(\tau_Q - t_0)/\tau} \frac{1 - \gamma(\eta)}{1 + \gamma(\eta)} e^{-\eta} d\eta. \quad (20)$$

The integral is now dominated by $\eta \gtrsim 0$, where $\gamma \approx 1$. Approximating the denominator $1 + \gamma \approx 2$, and substituting Eq. (6) for $\gamma(\eta)$ in the numerator, we obtain

$$n_3(\tau_Q) = \frac{1}{6} \left(\frac{\tau}{\tau_Q} \right)^\alpha \int_0^{(\tau_Q - t_0)/\tau} \eta^\alpha e^{-\eta} d\eta. \quad (21)$$

The upper limit of the integral can be replaced by ∞ in the $\tau_Q \gg \tau$ limit, the defect density at the end of cooling is then given by

$$n_3(\tau_Q) = \frac{\Gamma(1 + \alpha)}{6} \left(\frac{\tau}{\tau_Q} \right)^\alpha, \quad (22)$$

where $\Gamma(x)$ is the Gamma function. Importantly, here we show that the residual charge defects exhibit a scaling relation with the cooling rate with an exponent controlled by the exponent α of the cooling schedule. This result is also completely consistent with the power-law behavior obtained in our Glauber dynamics simulations, as shown by the dashed lines in Fig. 3.

In fact, the above argument can be applied to cooling schedules where the exponential factor admits a power-law expansion: $e^{-4\beta(t)J} = a(\tau_Q - t)^\alpha + \dots$ at $t \lesssim \tau_Q$. It is worth noting that, since either the Glauber or Metropolis dynamics for Ising spins is controlled by this Arrhenius factor, it is more natural to define cooling schedules in terms of this factor or equivalently the dimensionless parameter Eq. (4). The above series expansion of $e^{-4\beta J}$ corresponds to a physical temperature which vanishes in such a way that its inverse diverges logarithmically near $t = \tau_Q$:

$$T(t) \approx \frac{4J}{\alpha |\ln(\tau_Q - t)|}. \quad (23)$$

Finally, we note that nonuniversal behaviors, in particular nonpower-law dependencies, are expected for general cooling schedules that do not belong to this class. For example, for the linear in T cooling schedule: $T(t) \sim (1 - t/\tau_Q)$, which belongs to a special case of the so-called exponential cooling protocol, our Glauber dynamics simulations find a residual charge defect density which decays exponentially with cooling time: $n_3(\tau_Q) \sim \exp(-\text{const} \times \tau_Q)$. This result is consistent with the non-power-law behavior observed in the quench simulations of artificial colloidal kagome ice [50].

V. SUMMARY AND OUTLOOK

To summarize, we have presented a comprehensive study on the quench dynamics of nearest-neighbor kagome spin ice. This highly frustrated spin system is not only an important model in statistical physics and a representative system of geometrical frustration. The kagome spin ice exhibits an unusual nontopological defects, corresponding to triangle-simplexes which violate the ice-rule constraints, in the low temperature ice phase. The relaxation time that results from the decay of such nontopological solitons remains finite and nearly temperature independent. As a result, the standard KZ mechanism

cannot be applied to describe the quench dynamics of kagome ice. Yet, our extensive simulations and rate-equation analysis demonstrate that, for a special case of algebraic cooling protocols, the residual defect density in kagome spin ice exhibits a power-law relation with the cooling rate. We further show that the power-law dependencies result from the accumulation of excess defects during the nonadiabatic evolution at the late stage of cooling. Our analysis can also be extended to the quench dynamics of other systems with nontopological solitons.

The kagome spin ice considered in this work is an idealized frustrated Ising system with nearest-neighbor interactions. In realistic versions of kagome spin ice, either in magnetic compounds such as HoAgGe [40] and Dy₃Mg₂Sb₃O₁₄ [38,39] or in artificial nanomagnetic realizations [29–34], the magnetic Coulomb interaction between the background $Q = \pm 1$ magnetic charges leads to an intriguing intermediate phase where the charge degrees of freedom develop a long-range order, yet spins remain disordered [51,52]. The Coulomb interaction is minimized by a staggered charge distribution with all up-triangles assuming, e.g., $Q = +1$, while all down-triangles in the $Q = -1$ state, or vice versa. This charge ordered state can thus be described by an Ising order parameter $m = \langle Q_\Delta - Q_\nabla \rangle$. Importantly, phase transition into this charge ordered state thus belongs to the 2D Ising universality class [51,52]. As the temperature is further lowered, a long-range magnetic order with a tripled unit cell is eventually induced by the long-range dipole-dipole interaction. The corresponding magnetic transition is of the 2D three-state Potts universality class [52,53]. Nonequilibrium critical dynamics due to thermal quenches across these two phase transitions is expected to be well described by the KZ mechanism. A detailed investigation of kagome spin ice with dipolar interactions will be left for future study.

A rather different scenario occurs in the three-dimensional (3D) pyrochlore spin ice, and its 2D counterpart, the checkerboard spin ice. In both cases, the lattices are composed of simplexes (e.g., tetrahedra in the pyrochlore lattice) with four Ising spins. As a result, the ground-state manifold comprises 2-in-2-out simplexes with zero magnetic charge. Importantly, elementary excitations of such ice phases, i.e., simplexes that violate the 2-in-2-out ice rules, are topological in nature and carry a net magnetic charge, effectively behaving as emergent magnetic monopoles. Also contrary to the ice phase of kagome, both pyrochlore and checkerboard spin ices approaches a critical state as $T \rightarrow 0$, similar to the 1D Ising chain (however, unlike a 1D Ising chain, spins remain disordered at the $T = 0$ critical state in spin ice). This critical point in spin ices is unconventional as the correlation length diverges exponentially, instead of algebraically, when approaching zero temperature. Nonetheless, the KZ mechanism can be generalized to understand the nonequilibrium generation of topological defects when such spin ices are quenched to the critical point. A detailed account of the quench dynamics of pyrochlore spin ice will be presented elsewhere [54].

Finally, the presence of long-range dipolar interactions in the 3D pyrochlore spin ice induces a sharp first-order transition at very low temperatures [55]. The ground state below

the phase transition is a long-range spin ordered state with zero total magnetization. Since this magnetic transition is discontinuous, the standard KZ mechanism cannot be applied to this case. It is worth noting, however, that this ordered state is obtained by employing the nonlocal loop updates in Monte Carlo simulations [55]. As this magnetic phase transition occurs at a very low temperature, this magnetic ground state most likely cannot be reached through local spin dynamics, especially when the system already enters the nonadiabatic regime during a slow quench. Because of the ice-rules constraint, magnetization dynamics requires enough number of monopoles to activate the transition to the ordered states. For slow annealing processes, the system is likely to be frozen due to the extremely low number of monopoles at low temperatures. On the other hand, an interesting related subject is the kinetics of the magnetic transition when subjecting the pyrochlore spin ice to a sudden quench.

ACKNOWLEDGMENTS

The authors thank A. del Campo for useful discussions and Collaboration on related projects. The work was supported by the US Department of Energy Basic Energy Sciences under Contract No. DE-SC0020330. The authors also acknowledge the support of Research Computing at the University of Virginia.

APPENDIX: KIBBLE-ZUREK MECHANISM

The central idea of KZ mechanism is the breaking of adiabaticity due to critical slowing down when approaching a phase-transition point. Specifically, consider a general cooling schedule that starts at $t = 0$ and reaches the critical point at $t = \tau_Q$. Note that the same variable τ_Q is used in the case of kagome spin ice to denote the total time span of cooling from infinite temperature to $T = 0$, although the short-range kagome ice does not exhibit a critical point at

$T = 0$. However, for 3D pyrochlore and 2D checkerboard spin ices, the $T = 0$ does correspond to an unusual critical state with power-law spin correlations [54]. For thermal quenches across a critical point at T_c , the control parameter is given by

$$\epsilon(t) = [T_c - T(t)]/T_c. \quad (\text{A1})$$

The relaxation time τ of the system is now time-dependent through its dependence on $\epsilon(t)$. When the relaxation time $\tau(t)$ is shorter than the timescale $\epsilon/\dot{\epsilon}$ that characterizes the change of the control parameter, quasi-equilibrium can be quickly established and adiabaticity is maintained. The condition $\tau(t^*) = \epsilon/\dot{\epsilon}$ thus determines a freeze-out time t^* which signals the onset of nonadiabaticity. In the limit of slow cooling, a universal scaling relation for the freeze-out time $\hat{t} = \tau_Q - t^*$ (measured from the critical point) is obtained

$$\hat{t} \sim \tau_Q^{\nu z/(1+\nu z)}, \quad (\text{A2})$$

where ν is the exponent characterizing the power-law divergence of equilibrium correlation length $\xi \sim |T - T_c|^{-\nu}$, and z is the dynamical exponent $\tau \sim \xi^z$. Importantly, the residual density of topological defects can be estimated by the correlation length at the freeze-out time:

$$n_d \sim \hat{\xi}^{-D} \sim \tau_Q^{-D\nu/(1+\nu z)}, \quad (\text{A3})$$

where D is the spatial dimension of the system.

The KZ mechanism can also be generalized to describe nonequilibrium dynamics of the paradigmatic 1D Ising ferromagnet which exhibits an unconventional critical point at $T_c = 0$ [15–19]. Topological defects are kinks and antikinks that connect the doubly degenerate fully polarized ground states. Contrary to standard continuous phase transitions, both correlation length and relaxation time of the Ising chain diverge exponentially as $T \rightarrow 0$. Yet, a dynamical exponent can still be defined, e.g., $z = 2$ for Glauber dynamics, and a freeze-out time \hat{t} can be determined from the KZ condition $\tau(\tau_Q - \hat{t}) = \hat{t}$. However, while scaling relation is still obtained for the residual defect density, the exponent of the resultant power law depends on the cooling schedule.

-
- [1] A. Bray, Theory of phase-ordering kinetics, *Adv. Phys.* **43**, 357 (1994).
 - [2] *Kinetics of Phase Transitions*, edited by S. Puri and V. Wadhawan (CRC Press, Taylor & Francis Group, London, 2009).
 - [3] A. Onuki, *Phase Transition Dynamics* (Cambridge University Press, Cambridge, 2002).
 - [4] T. W. B. Kibble, Topology of cosmic domains and strings, *J. Phys. A: Math. Gen.* **9**, 1387 (1976).
 - [5] T. Kibble, Some implications of a cosmological phase transition, *Phys. Rep.* **67**, 183 (1980).
 - [6] W. H. Zurek, Cosmological experiments in superfluid helium? *Nature (London)* **317**, 505 (1985).
 - [7] W. Zurek, Cosmological experiments in condensed matter systems, *Phys. Rep.* **276**, 177 (1996).
 - [8] A. del Campo and W. H. Zurek, Universality of phase transition dynamics: Topological defects from symmetry breaking, *Int. J. Mod. Phys. A* **29**, 1430018 (2014).
 - [9] M. J. Harris, S. T. Bramwell, D. F. McMorrow, T. Zeiske, and K. W. Godfrey, Geometrical frustration in the ferromagnetic pyrochlore $\text{Ho}_2\text{Ti}_2\text{O}_7$, *Phys. Rev. Lett.* **79**, 2554 (1997).
 - [10] A. P. Ramirez, A. Hayashi, R. J. Cava, R. Siddharthan, and B. S. Shastry, Zero-point entropy in ‘spin ice’, *Nature (London)* **399**, 333 (1999).
 - [11] S. T. Bramwell and M. J. P. Gingras, Spin ice state in frustrated magnetic pyrochlore materials, *Science* **294**, 1495 (2001).
 - [12] *Spin Ice*, edited by M. Udagawa and L. Jaubert, Springer Series in Solid-State Sciences Vol. 197 (Springer-Verlag, Berlin, 2021).
 - [13] *Introduction to Frustrated Magnetism: Materials, Experiments, Theory*, edited by C. Lacroix, P. Mendels, and F. Mila, Springer Series in Solid-State Sciences Vol. 164 (Springer-Verlag, Berlin, 2011).
 - [14] R. Baxter, *Exactly Solved Models in Statistical Mechanics* (Dover, New York, 2008).

- [15] S. Suzuki, Cooling dynamics of pure and random Ising chains, *J. Stat. Mech.* (2009) P03032.
- [16] P. L. Krapivsky, Slow cooling of an Ising ferromagnet, *J. Stat. Mech.* (2010) P02014.
- [17] K. Jeong, B. Kim, and S. J. Lee, Nonequilibrium kinetics of excess defect generation and dynamic scaling in the Ising spin chain under slow cooling, *Phys. Rev. E* **102**, 012114 (2020).
- [18] Priyanka, S. Chatterjee, and K. Jain, Slow quench dynamics in classical systems: Kinetic Ising model and zero-range process, *J. Stat. Mech.* (2021) 033208.
- [19] J. J. Mayo, Z. Fan, G.-W. Chern, and A. del Campo, Distribution of kinks in an Ising ferromagnet after annealing and the generalized Kibble-Zurek mechanism, *Phys. Rev. Res.* **3**, 033150 (2021).
- [20] A. S. Wills, R. Ballou, and C. Lacroix, Model of localized highly frustrated ferromagnetism: The kagomé spin ice, *Phys. Rev. B* **66**, 144407 (2002).
- [21] R. F. Wang, C. Nisoli, R. S. Freitas, J. Li, W. McConville, B. J. Cooley, M. S. Lund, N. Samarth, C. Leighton, V. H. Crespi, and P. Schiffer, Artificial ‘spin ice’ in a geometrically frustrated lattice of nanoscale ferromagnetic islands, *Nature (London)* **439**, 303 (2006).
- [22] C. Nisoli, R. Moessner, and P. Schiffer, Colloquium: Artificial spin ice: Designing and imaging magnetic frustration, *Rev. Mod. Phys.* **85**, 1473 (2013).
- [23] S. H. Skjærvø, C. H. Marrows, R. L. Stamps, and L. J. Heyderman, Advances in artificial spin ice, *Nat. Rev. Phys.* **2**, 13 (2020).
- [24] G.-W. Chern, Artificial spin ice: Beyond pyrochlores and magnetism, in *Spin Ice*, edited by M. Udagawa and L. Jaubert (Springer-Verlag, Berlin, 2021), pp. 419–453.
- [25] M. Tanaka, E. Saitoh, H. Miyajima, T. Yamaoka, and Y. Iye, Magnetic interactions in a ferromagnetic honeycomb nanoscale network, *Phys. Rev. B* **73**, 052411 (2006).
- [26] Y. Qi, T. Brintlinger, and J. Cumings, Direct observation of the ice rule in an artificial kagome spin ice, *Phys. Rev. B* **77**, 094418 (2008).
- [27] E. Mengotti, L. J. Heyderman, A. F. Rodríguez, F. Nolting, R. V. Hügli, and H.-B. Braun, Real-space observation of emergent magnetic monopoles and associated Dirac strings in artificial kagome spin ice, *Nat. Phys.* **7**, 68 (2011).
- [28] S. Ladak, D. E. Read, G. K. Perkins, L. F. Cohen, and W. R. Branford, Direct observation of magnetic monopole defects in an artificial spin-ice system, *Nat. Phys.* **6**, 359 (2010).
- [29] S. Zhang, I. Gilbert, C. Nisoli, G.-W. Chern, M. J. Erickson, L. O’Brien, C. Leighton, P. E. Lammert, V. H. Crespi, and P. Schiffer, Crystallites of magnetic charges in artificial spin ice, *Nature (London)* **500**, 553 (2013).
- [30] L. Anghinolfi, H. Luetkens, J. Perron, M. G. Flokstra, O. Sendetskyi, A. Suter, T. Prokscha, P. M. Derlet, S. L. Lee, and L. J. Heyderman, Thermodynamic phase transitions in a frustrated magnetic metamaterial, *Nat. Commun.* **6**, 8278 (2015).
- [31] B. Canals, I.-A. Chioar, V.-D. Nguyen, M. Hehn, D. Lacour, F. Montaigne, A. Locatelli, T. O. Menteş, B. S. Burgos, and N. Rougemaille, Fragmentation of magnetism in artificial kagome dipolar spin ice, *Nat. Commun.* **7**, 11446 (2016).
- [32] A. Farhan, A. Scholl, C. F. Petersen, L. Anghinolfi, C. Wuth, S. Dhuey, R. V. Chopdekar, P. Mellado, M. J. Alava, and S. van Dijken, Thermodynamics of emergent magnetic charge screening in artificial spin ice, *Nat. Commun.* **7**, 12635 (2016).
- [33] W.-C. Yue, Z. Yuan, Y.-Y. Lyu, S. Dong, J. Zhou, Z.-L. Xiao, L. He, X. Tu, Y. Dong, H. Wang, W. Xu, L. Kang, P. Wu, C. Nisoli, W.-K. Kwok, and Y.-L. Wang, Crystallizing kagome artificial spin ice, *Phys. Rev. Lett.* **129**, 057202 (2022).
- [34] K. Hofhuis, S. H. Skjærvø, S. Parchenko, H. Arava, Z. Luo, A. Kleibert, P. M. Derlet, and L. J. Heyderman, Real-space imaging of phase transitions in bridged artificial kagome spin ice, *Nat. Phys.* **18**, 699 (2022).
- [35] K. Matsuhira, Z. Hiroi, T. Tayama, S. Takagi, and T. Sakakibara, A new macroscopically degenerate ground state in the spin ice compound $\text{Dy}_2\text{Ti}_2\text{O}_7$ under a magnetic field, *J. Phys.: Condens. Matter* **14**, L559 (2002).
- [36] Y. Tabata, H. Kadowaki, K. Matsuhira, Z. Hiroi, N. Aso, E. Ressouche, and B. Fåk, Kagomé ice state in the dipolar spin ice $\text{Dy}_2\text{Ti}_2\text{O}_7$, *Phys. Rev. Lett.* **97**, 257205 (2006).
- [37] T. Fennell, S. T. Bramwell, D. F. McMorrow, P. Manuel, and A. R. Wildes, Pinch points and Kasteleyn transitions in kagome ice, *Nat. Phys.* **3**, 566 (2007).
- [38] J. A. M. Paddison, H. S. Ong, J. O. Hamp, P. Mukherjee, X. Bai, M. G. Tucker, N. P. Butch, C. Castelnovo, M. Mourigal, and S. E. Dutton, Emergent order in the kagome Ising magnet $\text{Dy}_3\text{Mg}_2\text{Sb}_3\text{O}_{14}$, *Nat. Commun.* **7**, 13842 (2016).
- [39] Z. L. Dun, J. Trinh, K. Li, M. Lee, K. W. Chen, R. Baumbach, Y. F. Hu, Y. X. Wang, E. S. Choi, B. S. Shastry, A. P. Ramirez, and H. D. Zhou, Magnetic ground states of the rare-earth tripod kagome lattice $\text{Mg}_2\text{RE}_3\text{Sb}_3\text{O}_{14}$ (RE = Gd, Dy, Er), *Phys. Rev. Lett.* **116**, 157201 (2016).
- [40] K. Zhao, H. Deng, H. Chen, K. A. Ross, V. Petříček, G. Günther, M. Russina, V. Hutnanu, and P. Gegenwart, Realization of the kagome spin ice state in a frustrated intermetallic compound, *Science* **367**, 1218 (2020).
- [41] C. Castelnovo, R. Moessner, and S. L. Sondhi, Magnetic monopoles in spin ice, *Nature (London)* **451**, 42 (2008).
- [42] J. D. Bernal and R. H. Fowler, A theory of water and ionic solution, with particular reference to hydrogen and hydroxyl ions, *J. Chem. Phys.* **1**, 515 (1933).
- [43] L. D. C. Jaubert and P. C. W. Holdsworth, Signature of magnetic monopole and Dirac string dynamics in spin ice, *Nat. Phys.* **5**, 258 (2009).
- [44] R. J. Glauber, Time-dependent statistics of the Ising model, *J. Math. Phys.* **4**, 294 (1963).
- [45] P. L. Krapivsky, S. Redner, and E. Ben-Naim, *A Kinetic View of Statistical Physics* (Cambridge University Press, Cambridge, 2010).
- [46] E. Stoll, K. Binder, and T. Schneider, Monte Carlo investigation of dynamic critical phenomena in the two-dimensional kinetic Ising model, *Phys. Rev. B* **8**, 3266 (1973).
- [47] K. Binder and H. Müller-Krumbhaar, Investigation of metastable states and nucleation in the kinetic Ising model, *Phys. Rev. B* **9**, 2328 (1974).
- [48] T. Vojta, Chaotic behavior and damage spreading in the Glauber Ising model: A master equation approach, *Phys. Rev. E* **55**, 5157 (1997).
- [49] C. Castelnovo, R. Moessner, and S. L. Sondhi, Thermal quenches in spin ice, *Phys. Rev. Lett.* **104**, 107201 (2010).

- [50] A. Libál, A. del Campo, C. Nisoli, C. Reichhardt, and C. J. O. Reichhardt, Quenched dynamics of artificial colloidal spin ice, *Phys. Rev. Res.* **2**, 033433 (2020).
- [51] G. Möller and R. Moessner, Magnetic multipole analysis of kagome and artificial spin-ice dipolar arrays, *Phys. Rev. B* **80**, 140409(R) (2009).
- [52] G.-W. Chern, P. Mellado, and O. Tchernyshyov, Two-stage ordering of spins in dipolar spin ice on the kagome lattice, *Phys. Rev. Lett.* **106**, 207202 (2011).
- [53] G.-W. Chern and O. Tchernyshyov, Magnetic charge and ordering in kagome spin ice, *Philos. Trans. R. Soc., A* **370**, 5718 (2012).
- [54] Z. Fan, A. del Campo, and G.-W. Chern, Kibble-Zurek mechanism for nonequilibrium generation of magnetic monopoles in spin ices, [arXiv:2307.05267](https://arxiv.org/abs/2307.05267).
- [55] R. G. Melko, B. C. den Hertog, and M. J. P. Gingras, Long-range order at low temperatures in dipolar spin ice, *Phys. Rev. Lett.* **87**, 067203 (2001).